PAPER

Anomalous depinning of magnetic domain walls within the ferromagnetic phase of the Weyl semimetal $Co_3Sn_2S_2$

To cite this article: Zihao Shen *et al* 2023 *J. Phys.: Condens. Matter* **35** 045802

IOP Publishing Journal of Physics: Condensed Matter
J. Phys.: Condens. Matter **35** (2023) 045802 (7pp) https://doi.org/10.1088/1361-648X/aca57b

Anomalous depinning of magnetic domain walls within the ferromagnetic phase of the Weyl semimetal $Co_3Sn_2S_2$

Zihao Shen[1,*], X D Zhu[1,2], Rahim R Ullah[1], Peter Klavins[1] and Valentin Taufour[1,*]

[1] Department of Physics and Astronomy, University of California, Davis, CA 95616, United States of America
[2] Department of Optical Sciences and Engineering, Fudan University, Shanghai 200045, People's Republic of China

E-mail: xdzhu@physics.ucdavis.edu and vtaufour@ucdavis.edu

Received 7 October 2022, revised 7 November 2022
Accepted for publication 23 November 2022
Published 12 December 2022

Abstract

We report bulk magnetization measurements and spatially resolved measurements of magnetic domains in $Co_3Sn_2S_2$ single crystals. The results indicate that a previously reported magnetic anomaly around 130 K is due to an anomalous domain wall depinning upon cooling. Our measurements also reveal a hysteresis between field-cooled-cooling and field-cooled-warming magnetization curves acquired under a constant magnetic field below 300 Oe. This observation rules out the possibility that the anomaly stems from a second-order phase transition. Our results further suggest that changes in the shape of hysteresis loops from 5 to 170 K are caused by an unusual temperature-dependent domain nucleation field that changes sign around 130 K. The Kerr rotation images of the magnetic domains confirm that the domain walls depin between 120 and 140 K.

Keywords: magnetization, domain wall depinning, Kerr images, Weyl semimetal

(Some figures may appear in colour only in the online journal)

1. Introduction

Weyl Semimetals (WSMs) are material systems with non-degenerate bands that cross each other near the Fermi level when inversion symmetry or time-reversal symmetry is broken [1–3]. As one of the most interesting examples of WSM [4], $Co_3Sn_2S_2$ is a ferromagnetic material with a Curie temperature of $T_C = 174$ K [5]. The topological features of this material lead to a large anomalous Hall conductivity [6], an anomalous Nernst Hall effect [7], a negative magnetoresistance due to a chiral anomaly [4], and an unusual breaking-down of Ohm's law [8]. In addition, an unusually large magneto-optic effect has also been observed [9].

$Co_3Sn_2S_2$ crystallizes in a hexagonal lattice with triangular S and Sn layers interspersed between the kagome lattice planes of Co. The magnetic structure of this compound is still under investigation due to an anomaly in its magnetization occurring around 130 K upon cooling [10–16]. Various interpretations have been proposed to explain the anomaly. Wu *et al* proposed a hidden magnetic phase in $Co_3Sn_2S_2$ as revealed in AC susceptibility measurements [17]. Guguchia *et al* suggested an antiferromagnetic (AFM) phase in this compound based on two different muon precessions below T_C [18]. Meanwhile, other groups interpreted the anomaly as a spin glass transition [19, 20], a domain wall transition from linear domain walls to elliptical domain walls [21], and an enhanced domain wall motion observed by magnetic force microscopy [22]. Some of these proposals, however, have been challenged by experiments. For example, no strong evidence for an AFM phase was found in a neutron scattering experiment [13].

* Authors to whom any correspondence should be addressed.

In this context, we report bulk magnetization measurements on $Co_3Sn_2S_2$ single crystals in external magnetic fields applied along the c axis, where we find a depinning of magnetic domain walls around 130 K upon cooling and a hysteresis between field-cooled-cooling (FCC) and field-cooled-warming (FCW) magnetization at low fields. We also present magneto-optic Kerr effect (MOKE) images of magnetic domains in $Co_3Sn_2S_2$ from 120 to 140 K obtained under an external magnetic field of 94 Oe applied along the c axis. From the MOKE images, we extract fractions of single domains and domain walls near the magnetic anomaly around 130 K. While we find no strong evidence of sudden domain reorganization or domain size changes, we do find a change in domain fractions consistent with the partial depinning of magnetic domains. Our results indicate that the magnetic anomaly can be explained by a domain wall depinning effect. The origin of the domain wall depinning effect remains to be further investigated.

2. Methods

2.1. Single crystal growth

Single crystals of $Co_3Sn_2S_2$ were synthesized by solution growth [8, 23, 24]. A ternary mixture with initial composition $Co_{12}S_8Sn_{80}$ was first heated to 400 °C over 2 h and held there for another 2 h. It was then heated to 1050 °C over 6 h and held there for 10 h, followed by a slow, 90 h cool down to 740 °C. The remaining molten flux was removed by centrifugation. Shiny hexagonal crystals were obtained. The powder x-ray diffraction data refines to a hexagonal unit cell with $a = 5.3641(8)$ Å and $c = 13.1724$ Å, which are consistent with previously reported values [25].

2.2. Magnetization measurements and magnetic domain imaging

Magnetization measurements of $Co_3Sn_2S_2$ single crystals were performed in a Quantum Design MPMS SQUID up to 7 T with the magnetic field parallel to the c axis. Magnetization as a function of temperature was measured under various applied fields in both FCC and FCW conditions. Hysteresis loops were measured by first cooling down to the desired temperature in zero applied field and then sweeping the field. Before each measurement, we followed a demagnetization procedure to minimize the remanent field in the magnet and in the sample chamber by systematically oscillating the magnet to zero field at room temperature.

Polar MOKE images are acquired from as-grown $Co_3Sn_2S_2(0001)$ single crystal samples, using a normal-incidence Sagnac interferometric scanning microscope [26]. The microscope measures Kerr rotation as opposed to Kerr ellipticity [9]. It has a spatial resolution of 0.85 μm and a sensitivity of 4.4 μrad. The single crystal sample is mounted on a cold finger inside a cryostat. The sample is optically accessible from outside through an optical window. The temperature of the sample is variable from 300 to 5 K. We use a permanent magnet placed outside of the cryostat to produce a variable magnetic field of up to 100 Oe (0.01 T) along the c axis (the surface normal) of the sample. For this experiment, the field is held constant at 94 Oe, measured by a Hall effect sensor.

3. Results and discussion

3.1. Magnetization measurements

The FCC curve with a magnetic field of 1000 Oe applied parallel to the c axis is shown in figure 1, and illustrates the ferromagnetic-paramagnetic transition. The inverse susceptibility is fit to the Curie–Weiss law and we obtain an effective moment of 1.14 μ_B per Co and a Curie–Weiss temperature of $\theta_{CW} = 175$ K, which are consistent with previously published work [4, 23, 25, 27]. There is no difference in the FCC and FCW magnetization at fields above 300 Oe. If the applied field is below 300 Oe, however, two anomalies emerge. First, the FCC and FCW curves start to deviate near T_C. Second, a local maximum arises at $T_A \approx 130$ K in the FCC data, which is also reported in other studies [10–16, 18]. The local maximum disappears above 300 Oe and below 50 Oe, while a small hysteresis between FCC and FCW still remains at 50 Oe. The field dependence of T_A is relatively small, as shown in the inset of figure 1(b). The fact that the anomaly disappears above 300 Oe, where the magnetization is saturated, suggests its origin is related to magnetic domains. A local minimum also emerges in the FCW magnetization albeit at higher temperature. The hysteresis between FCC and FCW magnetizations indicates it is unlikely that the local maximum and minimum in the FCC and FCW magnetization are due to a second order phase transition, which should not depend on magnetic history.

We will compare the fraction of magnetic domains assuming no pinning with the fraction extracted from our experimental magnetization where pinning effects are inevitable. In the absence of domain wall pinning, the demagnetising field $H_d = N_c M$ perfectly counteracts the applied field, $H_{applied}$, as long as $H_{applied} < N_c M_s$. N_c is the demagnetization factor along the c-direction. Because the c axis is the easy magnetization axis, N_c can be measured experimentally from a plot of M^2 versus $H_{applied}/M$ for the $M(H)$ data along the easy axis of magnetization as shown in figure 2(c). The x-intercept gives the value of the demagnetization factor along the easy magnetization axis [28, 29]. Due to the existence of domain pinning, the curves at low temperatures tend to shift to the right. Therefore, we used the x-intercept at 170 K, where domain pinning is negligible, as the demagnetization factor and obtained $N_c = 0.608$. M_s is the spontaneous magnetization, which is obtained from the extrapolation to zero field of $M(H)$ curves, as shown in figures 4(c) and (d). The magnetization of the sample can be related to the fraction of up domains $n_\uparrow$, where $M = (2n_\uparrow - 1)M_s$. From $H_{applied} = N_c M$, we can determine $n_\uparrow$ as follows:

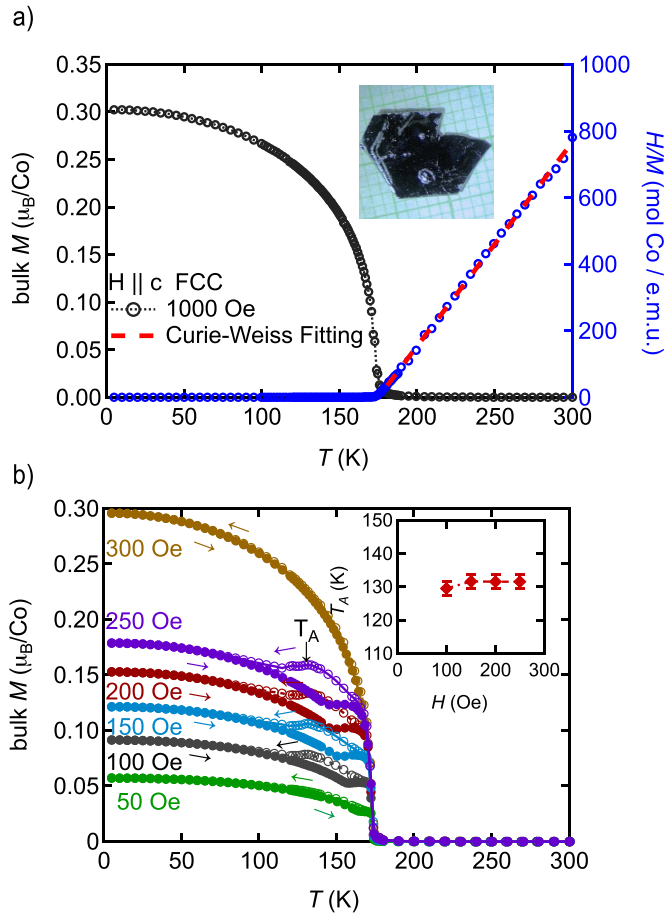

Figure 1. (a) Magnetization as a function of temperature measured by FCC in a 1000 Oe applied field parallel to the c axis. The blue curve shows a Curie–Weiss fitting with an effective moment 1.14 μ_B per Co. The inset shows a $Co_3Sn_2S_2$ single crystal grown from solution growth. (b) FCC and FCW curves show a hysteresis between 100 K and $T_C = 174$ K. T_A is the temperature of the magnetic anomaly where the FCC magnetization reaches a local maximum followed by a downward kink. The inset shows the field dependence of T_A.

$$n_{\uparrow} = \frac{1}{2M_s}\frac{H_{\text{applied}}}{N_c} + \frac{1}{2}. \tag{1}$$

The applied field, H_{applied}, and the demagnetization factor, N_c, are temperature independent. Equation (1) gives us the result that, without pinning, the fraction of up domains should decrease as temperature decreases because M_s increases.

In figure 2(a) we compare the calculated fraction of magnetically aligned (up) domains with the value deduced from the experimental magnetization. The blue and red curves are the temperature dependence of the up-domain fraction extracted from the FCC and FCW magnetization respectively at 100 Oe, with the following formula:

$$n_{\uparrow} = \frac{M}{2M_s} + \frac{1}{2}. \tag{2}$$

The black curve is the fraction of up-domain calculated from a demagnetization theory [30] in equation (1). We can see that domain wall pinning keeps the up-domain fraction above the

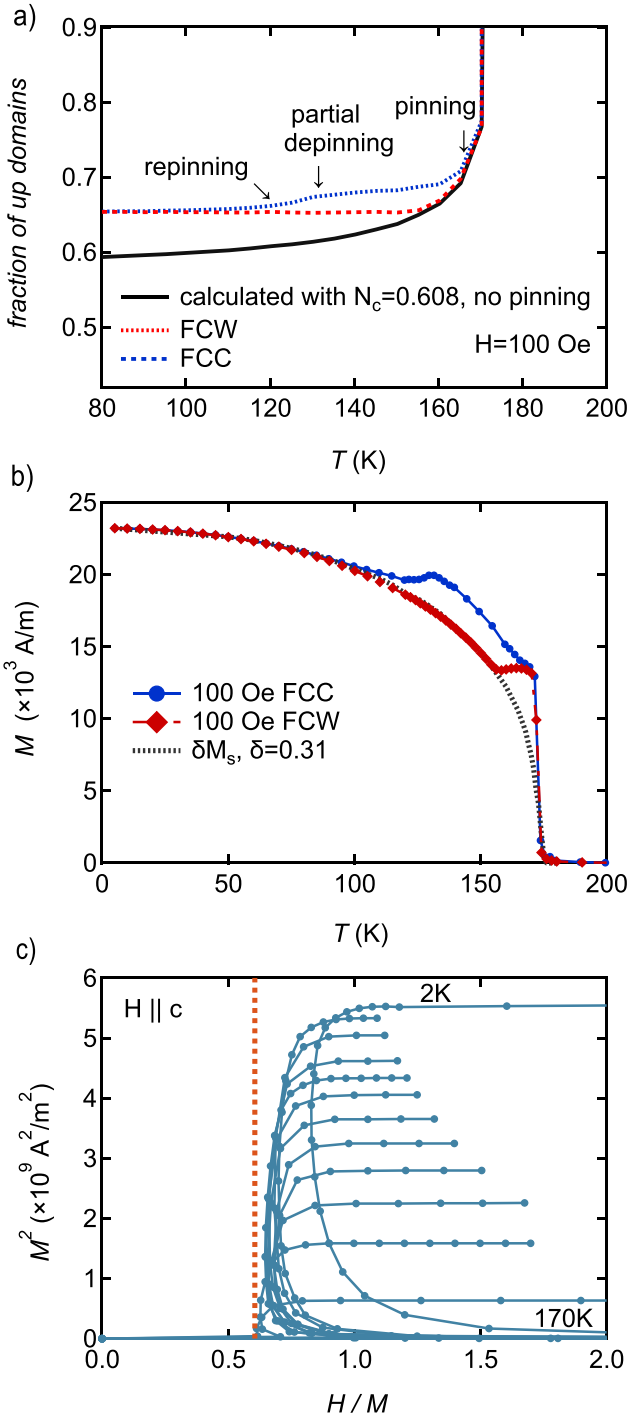

Figure 2. (a) Temperature dependence of the fraction of up domains extracted from FCC (blue curve) and FCW (red curve) magnetization data at $H = 100$ Oe compared to our model based on demagnetization theory with $N_c = 0.608$ (black curve). (b) Comparison between FCC and FCW magnetization at 100 Oe and δM_s with $\delta = 0.31$. (c) M^2 versus H/M at various temperatures. The intercept on the x-axis (orange line) reveals a demagnetization factor N_c of 0.608.

theoretical value for all but the temperatures near T_C. While cooling down below T_C, the system encounters a domain-wall pinning effect where the blue curve begins to deviate from the black curve. This domain-wall pinning causes

the magnetization to increase nearly proportionally to M_s as shown by the blue curve in figure 2(b). Below around 132 K, the system enters a partial depinning region where the up-domain fraction decreases toward its theoretical no pinning value. The magnetization consequently decreases, which causes a local maximum near 132 K. Upon further cooling, there is a competition between this anomalous depinning effect and the reduced thermal energy which tends to favor pinning. The reduced thermal energy eventually dominates around 120 K and domain walls tend to pin again. Therefore, the magnetization tends to be proportional to M_s, i.e. $M = \delta M_s$ with $\delta = 0.31$. The repinning is consistent with the fact that domain walls in $Co_3Sn_2S_2$ rarely move below 119 K as reported by a Lorentz microscopy study [31]. Upon warming up, as shown by the red curve in figure 2, since domain walls are pinned, the domain fraction remains unchanged until around 155 K, where the increased thermal energy allows more up domains to form. Due to the presence of domain-wall pinning, the total magnetization of the sample when cooled down and warmed up follows two different pathways, resulting in the hysteresis between the FCC and FCW magnetization curves.

For evidence of domain-wall depinning effects, we measured hysteresis loops with the applied field only up to 100 Oe at various temperatures. An example is shown in figure 3(a). We note that domain structures depend on defects and the shape of a sample [32, 33]. For this reason, we use the same sample for all the bulk magnetization measurements presented in this article. The virgin curve at 130 K remains flat at first, then increases with a constant slope, which is the hallmark of a domain-wall pinning-type virgin curve [30]. The magnetization of the field-increasing part of the hysteresis loop is smaller than that of the virgin curve, indicating that the domains encounter some pinning effect. Asymmetry between positive and negative coercive field emerges up to 160 K. The asymmetry can be attributed to the exchange bias, which has been observed by other groups [19, 34], or the remanent field during the measurement. At 130 K, the negative coercive field is $H_c^- = -34.3(5)$ Oe, while the positive coercive field is $H_c^+ = 42.1(3)$ Oe, and the actual coercive field, H_c, is taken to be the average of the absolute value of the two. The nucleation field $H_{nuc}^{\downarrow}$, below which the down domains start to form, was obtained as shown in figure 3(a). If there were no domain-wall pinning, the $M(H)$ curve should be a straight line. Therefore, the coercive field should always be zero and the nucleation field $H_{nuc}^{\downarrow}$ should be the highest field of the hysteresis loop, i.e. 100 Oe. However, figure 3(b) reveals a local maximum of H_c and a local minimum of $H_{nuc}^{\downarrow}$ at 132 K, below which H_c starts to decrease and $H_{nuc}^{\downarrow}$ starts to increase, indicating a partial domain-wall depinning. The domain wall depinning around 130 K is consistent with the high mobility of domain walls observed near 130 K with a magnetic force microscope [22]. Further below 120 K, domain-wall pinning strength increases again. H_c consequently increases and $H_{nuc}^{\downarrow}$ decreases. We note that the local maximum disappears at fields above 300 Oe. As shown in figure 5, 300 Oe is the largest value of the nucleation field when this sample is fully magnetized. Therefore, down domains cannot form above 300 Oe and the local maximum

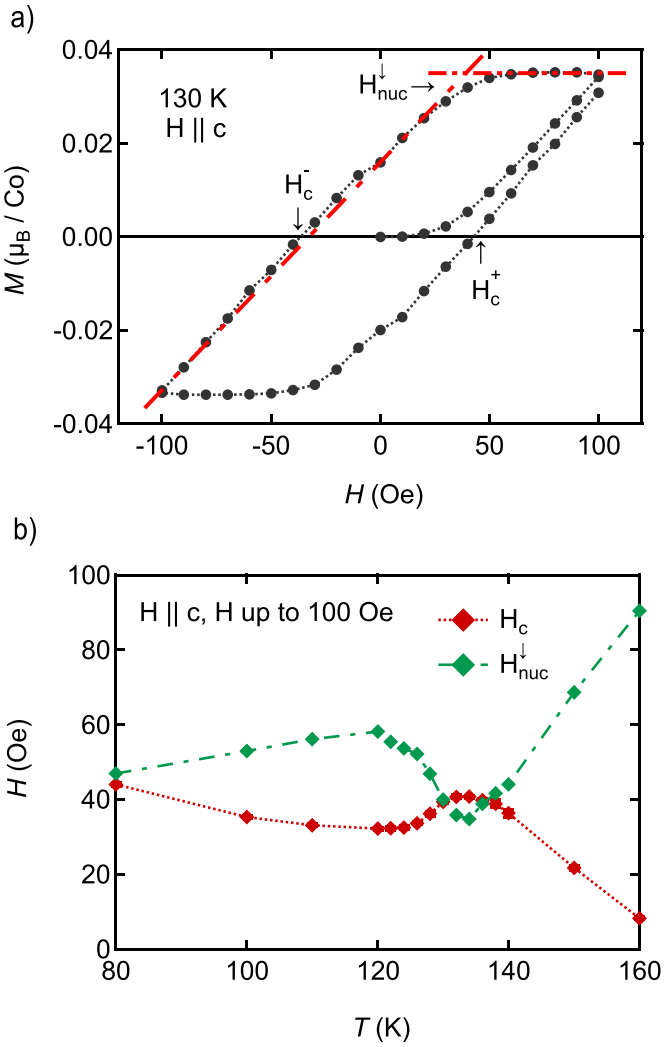

Figure 3. (a) Hysteresis loop with applied field parallel to the c axis up to 100 Oe. The arrow shows the coercive field H_c. Nucleation field $H_{nuc}^{\downarrow}$ is obtained by the intersection of red lines. (b) H_c and $H_{nuc}^{\downarrow}$, with maximum field up to 100 Oe, as a function of temperature.

disappears. The actual value of the nucleation field depends on the shape of the sample and defects [32, 33]. Although the field above which the local maximum in the FCC curve disappears varies among different samples, the depinning around 130 K is a general observation in this compound [10–16, 18]. While domain-wall pinning upon cooling is very common in many systems, depinning upon cooling is anomalous. The origin of the depinning, however, is still under investigation. It is possible that the depinning is enabled by the recently observed local structure distortion [20] which can reduce the local anisotropy energy and thus allows domains to flip, causing the depinning around 130 K.

Since the sample is single domain at high fields, one can wonder if there is still evidence for the magnetic anomaly in the hysteresis loops up to 7 T. As shown in figure 4, the spontaneous magnetization, M_s, is about 0.3 μ_B/Co at 5 K [6, 25]. We also found that increasing temperature causes

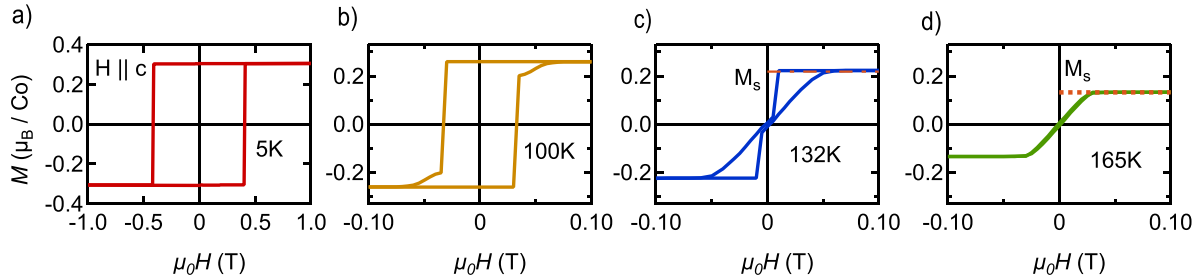

Figure 4. Hysteresis loops with the applied field up to 7 T parallel to the c axis at various temperatures. Only a selection of temperatures are shown. The hysteresis gradually changes from rectangle to bi-triangular shape. Spontaneous magnetization M_s is obtained as shown in (c) and (d).

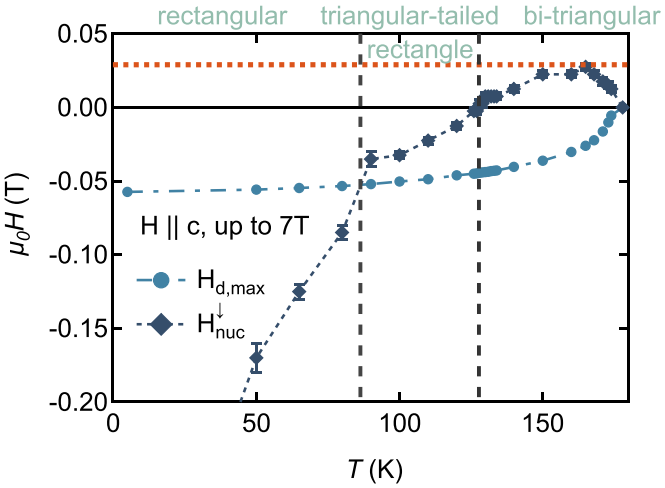

Figure 5. Temperature dependence of nucleation field and maximum demagnetization field. The red dashed line shows the 300 Oe field.

the shape of the hysteresis loop to change from a rectangular shape (5 K), to a triangular-tailed rectangle (100 K), to a bi-triangular shape (132 K), until the hysteresis disappears completely (160 K). The change from triangular-tailed-rectangle to rectangular shape of hysteresis loops can be explained with a domain-wall motion model. As shown in figure 5, the magnitude of the nucleation field increases as cooling down, until, around 85 K, it exceeds the magnitude of the demagnetization field, causing the hysteresis loop changes from a triangular-tailed shape to a rectangular shape [35]. While there is no minimum in the nucleation field, we find that the nucleation field changes its sign around 130 K, causing the hysteresis loop changes from a bi-triangular shape to a triangular-tailed shape.

3.2. Magnetic domain structures from 140 to 120 K

Except for a recent MOKE study reported by Lee and coworkers [21], domain structures of $Co_3Sn_2S_2(0001)$ single crystal samples are largely unknown. By measuring spatially resolved magnetization through the Kerr effect as a function of temperature, we can examine whether the magnetic anomaly is intrinsic to the physics in a single domain, or, as we suggested previously, is due to the presence of multiple domains and

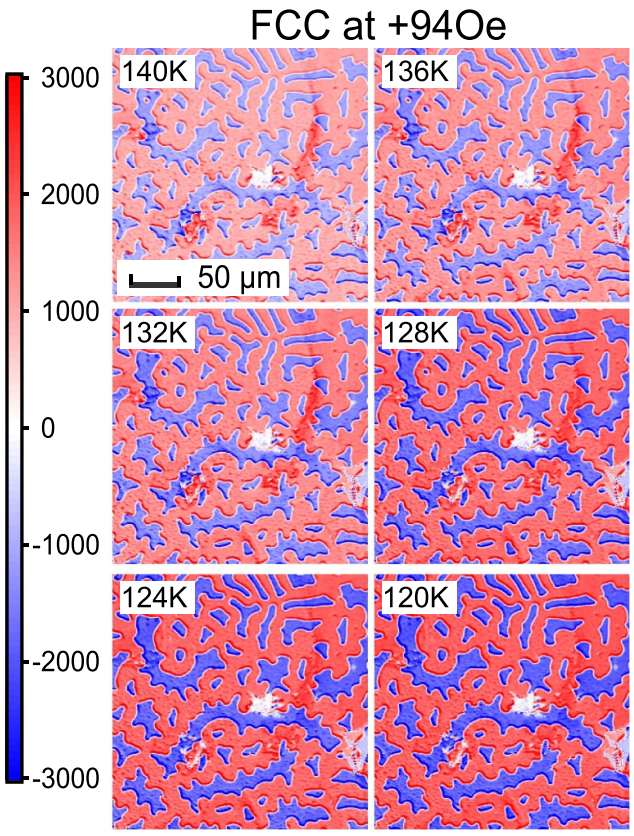

Figure 6. Polar Kerr rotation images of $Co_3Sn_2S_2(0001)$ after FCC in $H_{||} = +94$ Oe (pointing out of paper along the c-axis) from room temperature acquired at (a) 140 K; (b) 136 K; (c) 132 K; (d) 128 K; (e) 124 K; (f) 120 K. Red regions are domains with magnetization pointing out of paper along the direction of the applied magnetic field; blue regions are domains with magnetization pointing in the opposite direction. The unit of Kerr rotation is μrad. The scale bar is 50 μm. The image size is 240 μm $\times$ 240 μm.

domain walls. Such detailed information is elusive from bulk measurements averaged over the entire sample.

To examine the domain structures near $T = 130$ K, we acquired a set of MOKE images at 140, 136, 132, 128, 124, and 120 K after the sample is field cooled in a magnetic field of $H_{||} = +94$ Oe. These images are shown in figure 6. Other than the disappearance of a small embedded red domain in the upper left corner (between 136 and 132 K) and that of

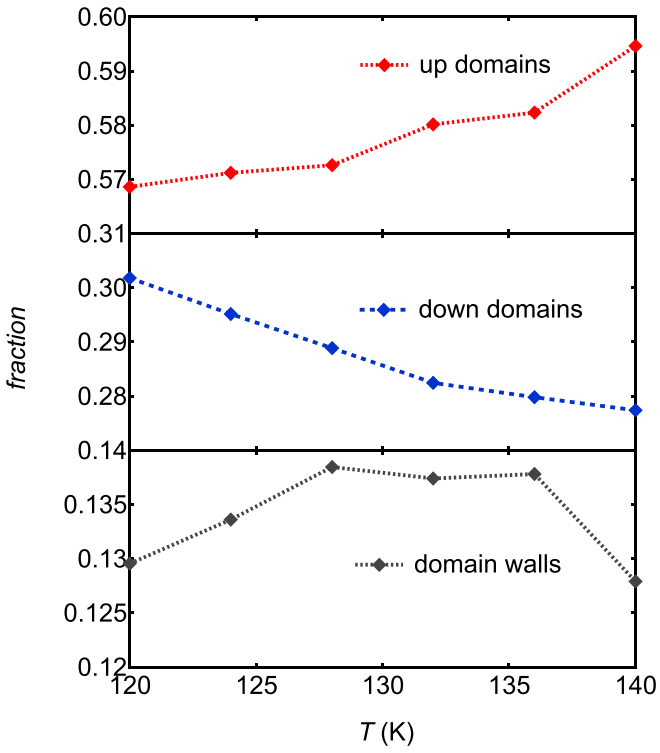

Figure 7. Evolution of the fraction of up and down domains and domain walls while cooling down extracted from MOKE images. The fraction of up domains shrinks while the fraction of down domains grows.

an embedded blue domain to its immediate right (between 128 and 124 K), the domain structure remains essentially unchanged between 140 and 120 K. Limited by the spatial resolution of the scanning microscope (0.85μm), from these MOKE images alone, we cannot rule out transitions that involve domain walls, such as those proposed in [21].

We extract the fraction of up domains, down domains, and domain walls from these images as follows. First, we measure the average absolute Kerr rotation of up and down domains. Then, we count points above 75% of the average value as up or down domains, and points below that value as domain walls. Figure 7 shows the evolution of these fractions as a function of temperature. As the sample is cooled down, the fraction of up domains shrinks while that of down domains grows due to the demagnetization effect. The fact that the temperature variation of the domain fractions follows the same trend as the evolution expected from the case with no pinning confirms that the magnetic domain walls are indeed able to move between 120 and 140 K.

4. Conclusion

We find that the hysteresis between FCC and FCW magnetization in low fields is due to a domain-wall pinning effect and attribute the magnetic anomaly T_A near 130 K in the FCC magnetization curve in $Co_3Sn_2S_2$ to an anomalous domain wall depinning effect upon cooling. We also find that the nucleation field changes its sign around the anomaly temperature $T_A = 130$ K, causing the shape of the hysteresis loops to change from triangular-tailed rectangles into double-triangles. The MOKE images also reveal a magnetic domain walls depinning between 140 and 120 K upon cooling. Our findings corroborate some other domain studies in this compound [22, 31]. However, the origin the domain-wall depinning still requires further investigation.

5. Acknowledgments

V T, Z S and R R U acknowledge support from the UC Lab Fees Research Program (LFR-20-653 926) and UC Davis Startup funds. X D Z acknowledges a Visiting Lecture Professorship from Fudan University in support of this work. We acknowledge support from the Physics Liquid Helium Laboratory fund.

Data availability statement

The data generated and/or analysed during the current study are not publicly available for legal/ethical reasons but are available from the corresponding author on reasonable request.

ORCID iD

Zihao Shen https://orcid.org/0000-0002-5937-7027

References

[1] Wan X, Turner A M, Vishwanath A and Savrasov S Y 2011 *Phys. Rev.* B **83** 205101
[2] Burkov A A and Balents L 2011 *Phys. Rev. Lett.* **107** 127205
[3] Armitage N P, Mele E J and Vishwanath A 2018 *Rev. Mod. Phys.* **90** 015001
[4] Liu E *et al* 2018 *Nat. Phys.* **14** 1125–31
[5] Yan W, Zhang X, Shi Q, Yu X, Zhang Z, Wang Q, Li S and Lei H 2018 *Solid State Commun.* **281** 57–61
[6] Wang Q, Xu Y, Lou R, Liu Z, Li M, Huang Y, Shen D, Weng H, Wang S and Lei H 2018 *Nat. Commun.* **9** 1–8
[7] Yang H *et al* 2020 *Phys. Rev. Mater.* **4** 024202
[8] Nagpal V and Patnaik S 2020 *J. Phys.: Condens. Matter* **32** 405602
[9] Okamura Y *et al* 2020 *Nat. Commun.* **11** 1–8
[10] Kassem M A, Tabata Y, Waki T and Nakamura H 2017 *Phys. Rev.* B **96** 014429
[11] Kassem M A, Tabata Y, Waki T and Nakamura H 2020 *J. Phys.: Condens. Matter.* **33** 015801
[12] Zhang Q, Okamoto S, Samolyuk G D, Stone M B, Kolesnikov A I, Xue R, Yan J, McGuire M A, Mandrus D and Tennant D A 2021 *Phys. Rev. Lett.* **127** 117201
[13] Soh J R, Yi C, Zivkovic I, Qureshi N, Stunault A, Ouladdiaf B, Rodríguez-Velamazán J A, Shi Y, Rnnow H M and Boothroyd A T 2022 *Phys. Rev.* B **105** 094435
[14] Shin D H, Jun J H, Lee S E and Jung M H 2021 (arXiv:2105.03892)
[15] Hu J, Kan X, Chen Z, Zheng G and Ma Y 2022 *J. Am. Ceram. Soc.* **105** 4827–39
[16] Shen J *et al* 2019 *Appl. Phys. Lett.* **115** 212403
[17] Wu H, Sun P, Hsieh D, Chen H, Kakarla D C, Deng L, Chu C and Yang H 2020 *Mater. Today Phys.* **12** 100189
[18] Guguchia Z *et al* 2020 *Nat. Commun.* **11** 1–9

[19] Lachman E, Murphy R A, Maksimovic N, Kealhofer R, Haley S, McDonald R D, Long J R and Analytis J G 2020 *Nat. Commun.* **11** 1–8
[20] Zhang Q, Zhang Y, Matsuda M, Garlea V O, Yan J, McGuire M A, Tennant D A and Okamoto S 2022 *J. Am. Chem. Soc.* **144** 14339–50
[21] Lee C, Vir P, Manna K, Shekhar C, Moore J, Kastner M, Felser C and Orenstein J 2022 *Nat. Commun.* **13** 1–6
[22] Howlader S *et al* 2020 *J. Phys.: Condens. Matter.* **33** 075801
[23] Lin X, Bud'ko S L and Canfield P C 2012 *Phil. Mag.* **92** 2436–47
[24] Kassem M A, Tabata Y, Waki T and Nakamura H 2015 *J. Cryst. Growth* **426** 208–13
[25] Vaqueiro P and Sobany G G 2009 *Solid State Sci.* **11** 513–18
[26] Zhu X 2021 *AIP Adv.* **11** 085214
[27] Schnelle W, Leithe-Jasper A, Rosner H, Schappacher F M, Pöttgen R, Pielnhofer F and Weihrich R 2013 *Phys. Rev.* B **88** 144404
[28] Lamichhane T N, Taufour V, Thimmaiah S, Parker D S, Bud'ko S L and Canfield P C 2016 *J. Magn. Magn. Mater.* **401** 525–31
[29] Arrott A 1957 *Phys. Rev.* **108** 1394–6
[30] de Lacheisserie E du T, Gignoux D and Schlenker M (eds) 2004 *Magnetism Fundamentals* (Berlin: Springer)
[31] Sugawara A, Akashi T, Kassem M A, Tabata Y, Waki T and Nakamura H 2019 *Phys. Rev. Mater.* **3** 104421
[32] Vial F, Joly F, Nevalainen E, Sagawa M, Hiraga K and Park K 2002 *J. Magn. Magn. Mater.* **242** 1329–34
[33] Zeper W, Van Kesteren H, Jacobs B, Spruit J and Carcia P 1991 *J. Appl. Phys.* **70** 2264–71
[34] Noah A *et al* 2022 *Phys. Rev.* B **105** 144423
[35] Tsymbal L, Kakazei G and Bazaliy Y B 2009 *Phys. Rev.* B **79** 092414